Temperature dependence of disorder sensitivity of phonon modes in finite-gap materials

Omkar V. Rambadey,* Kailash Kumar, and Pankaj R. Sagdeo†
Materials Research Laboratory, Department of Physics, Indian Institute of Technology Indore, Indore 453552, Madhya Pradesh, India

(Received 13 December 2023; revised 12 June 2024; accepted 15 November 2024; published 3 December 2024)

The correlation between electronic disorder (quantified by the Urbach energy E_U) and phonon linewidth (Γ) is known to be linear. However, both parameters exhibit temperature dependence, raising the question of whether the slope of the Γ vs E_U plot remains constant with temperature. In this study, we investigate temperature dependence of the slope, denoted as ξ, which represents the sensitivity of phonon mode to changes in disorder. By applying theoretical models for the temperature dependence of Γ and E_U, we derive an expression for $\xi(T)$, revealing its nonlinear behavior at varying temperatures. Our analysis, based on Raman and optical absorption spectra of $EuFeO_3$, demonstrates the explicit temperature dependence of ξ. This provides insights into the disorder sensitivity of vibrational modes, which is crucial for understanding phonon dynamics and transport properties. The findings are further supported by additional investigations on TiO_2, emphasizing the utility of combined optical and Raman spectroscopic techniques in probing phonon-resolved disorder sensitivity in materials with finite bandgap where E_U can be observed.

DOI: 10.1103/PhysRevB.110.235201

I. INTRODUCTION

The quantized lattice vibrations (phonon) are known to govern not only thermal and structural properties [1–3], but also electronic structures in materials through electron-phonon interactions [4,5]. It involves transport in insulators, conductors, and even in superconductors [6,7]. In that view, the important physical properties may have a correlation with particular phonon mode(s) [8–10] where the investigation of selective excitation of phonons becomes crucial [10,11]. However, multiple phonon modes are excited at once via the thermal excitation of the sample; hence, to excite the target mode, coherent phonon spectroscopy technique is utilized [12]. Nevertheless, it is noteworthy that the susceptibility of phonon modes towards the lattice perturbations can affect their response to the excitation. Therefore, it can be an important aspect to look into the sensitivity of phonon modes towards the disorder associated with lattice in which thermal disorder can be a crucial factor. In that regard, the temperature-dependent (TD) spectroscopic study is although not a new approach but is very important when it comes to understanding the insights of a system [4,13–16]. It is known that the increase of the sample temperature would enhance the amplitude of vibration [17–20]. The resulting increased average amplitude of the lattice oscillations may not be isotropic in nature throughout the entire lattice environment and the anharmonicity, thus introduced, in lattice can ultimately affect the phonon lifetime (τ), such that the enhanced scattering processes eventually lead to decrease τ [21,22]. This can be efficiently observed in the Raman spectra of the materials [23–27]. Indeed, the broadened peaks advocate the reduced τ in accordance with the relation [28]

$$\frac{1}{\tau} \sim \frac{\Delta E}{\hbar} \propto \Delta\omega \propto \Gamma. \tag{1}$$

The quantity ΔE ($\Delta\omega$) relates to the spectral width (linewidth Γ) of the phonon mode observed in the Raman spectra of the sample, which emphasizes inverse relation with τ. The presence of disorder can alter the coherent phonon propagation in the crystal lattice, attributing to reduced τ, hence broadened phonon modes as probed via light-matter interaction, such as Raman spectroscopic technique [29–33].

Moreover, the lattice disorder cannot only affect the phonon characteristics, but also the electronic structure. As the disorder can have chemical (elemental substitution) or thermal (temperature variation) origin, this can introduce spatial potential fluctuations in the lattice [34], eventually leading to the finite spread in the energy and momentum of the electrons attributing to the manifestation of faint states near the band edges, also known as Urbach tail states [35,36]. The collective width of this band is termed as Urbach energy (E_U), and quantifies the overall disorder in the system. Experimentally, the existence of these states can be prominently realized in the optical absorption spectra of semiconductors [37]. For this, the Urbach rule [35,38] gives a method for the estimation of E_U by considering the exponential behavior of the absorption coefficient below the fundamental absorption edge [37,39,40], wherein E_U is obtained from fitting the exponential portion of the absorption coefficient near the band edge [36,41]. Since both the parameters E_U and the phonon linewidth (Γ) contain the information of the overall disorder [42–45], a correlation can be anticipated to exist between these two. For instance, the experimentally observed temperature variation of Γ and E_U follow a similar trend of evolution, as observed for several systems [23,46,47]. Furthermore, the covariation of E_U and Γ has also been observed in various systems, viz., in the report by Huso *et al.* [48] on Mg-substituted ZnO system, in $PrFe_{1-x}Cr_xO_3$ system as

*Contact author: ovrambadey@gmail.com
†Contact author: prs@iiti.ac.in

reported by Kumar *et al.* [25] as a result of chemical disorder, and also for thermal disorder introduced into $EuFeO_3$ [49] and $BaTiO_3$ [50] systems, which emphasize the correlation between these two quantities. In spite of having information in the literature, the analytical discussion on this correlation is limited. Apart from the variation in E_U and Γ because of chemical/substitutional disorder, the mathematical interpretation for the temperature variation of these quantities is well known in the literature [21,38,43,51]. So, the current paper also emphasizes on the temperature-dependent studies. For instance, the Einstein oscillator model is well adopted to explore the temperature variation of E_U [13,43,44,52],

$$E_U(T) = E_{01} + \frac{E_{02}}{\exp(\Theta_E/T) - 1}; \Theta_E = \frac{\hbar\omega_E}{k_B}, \tag{2}$$

where ω_E is the Einstein frequency, and the collective term $\hbar\omega_E/k_B$ is recognized as Einstein temperature Θ_E. The parameter E_{01} is the static part and relates to the temperature-independent contribution, E_{02} is the coefficient of the dynamic part.

Similarly, the temperature dependence of $\Gamma(T)$ is defined for three-phonon process (3ph) via the relation [23]

$$\Gamma(T)_{3-ph} = \Gamma_0 + \frac{2\Gamma_0}{\exp\left(\frac{\hbar\omega_0}{2k_BT}\right) - 1}, \tag{3}$$

where, Γ_0 and ω_0 correspond to the width, and the Raman shift at $0K$, respectively. It is basically related to the anharmonic effects on the phonon lineshape that causes the symmetric broadening of Raman mode profile. Furthermore, in 1983, Balkanski, Wallis, and Haro showed that extending the above model to the four-phonon process (4ph) provides more satisfactorily reasonable agreement with the experimental data, which is given by [21]

$$\Gamma(T)_{4-ph} = \Gamma_{01}\left(1 + \frac{2}{\exp\left(\frac{\hbar\omega_0}{2k_BT}\right) - 1}\right) + \Gamma_{02}\left(1 + \frac{3}{\exp\left(\frac{\hbar\omega_0}{3k_BT}\right) - 1} + \frac{3}{\left(\exp\left(\frac{\hbar\omega_0}{3k_BT}\right) - 1\right)^2}\right). \tag{4}$$

Here, the constant multipliers Γ_{01} and Γ_{02} relate to the contribution at 0 K. The first term here may resemble that from the 3ph process such that the second term appearing to be the contribution because of 4ph process, or else, the 3ph process may seem as a subprocess for the case of 4ph scattering; nevertheless, these processes will exist simultaneously in a system so that the Γ_{4-ph} represents the total contribution of these processes as a whole [21]. So, the discussion on 4ph process in this paper will refer to the above equation as a whole and not as the extra-apparent second term.

The similar mathematical manifestations of the functional forms of $E_U(T)$ and $\Gamma(T)$ has been a motivation to explore the mentioned correlation analytically. Such a correlation has been identified empirically in an earlier report [26], further explored in other semiconductor oxide systems [49,50], and has the form

$$\Gamma = \xi E_U + \lambda \tag{5}$$

where ξ and λ were discussed to be material-specific coefficients found by fitting the experimental data. The Γ of a phonon mode is observed to evolve linearly with respect to E_U of the system, and so the form of the empirical relation in Eq. (5), providing ξ as the slope of the linear plot; such a linear trend was found to hold for variety of samples [26,49,50]. Because the Urbach tail is observable owing to the finite-energy gap and Raman signals are not overridden by charge density as in metals, studying this correlation and hence parameter ξ is feasible with semiconductor and dielectric samples. A linear behavior suggests constant nature of the slope ξ; however, as both Γ and E_U are temperature-dependent quantities, it further raises the curiosity to explore the constant nature of the slope of experimentally observed Γ vs E_U linear plot [26,49,50], because it can provide the information of the disorder sensitivity of the phonon mode.

In this paper, we investigate this question through analytical means. In Sec. III, we revisit the empirical relation [Eq. (5)], and attempt to obtain the functional form for the parameter $\xi(T)$ with the help of the above-elaborated models. Later, in the Discussions section, we visualize the results through a comparison of experimental and theoretical outcomes on the two different physical systems, viz., $EuFeO_3$ and TiO_2, describing the temperature dependence of the disorder sensitivity along with discussing the mystery of linear of Γ vs E_U behavior in the vicinity of room temperature. It turns out that the Einstein temperature plays a role in governing this variation thereby the sensitivity ξ. In order to further extend the discussion on another system, anatase TiO_2 is considered as $\Theta_E^{TiO_2} > \Theta_E^{EuFeO_3}$ [41,53,54]. It possesses D_{2h} symmetry such that the Ti-O cage in its anatase phase exhibits finite distinct Raman active bands around 140 cm^{-1}, 196 cm^{-1}, 396 cm^{-1}, 515 cm^{-1}, and 640 cm^{-1}. Although the bandwidth of the $\sim$ 515 cm^{-1} feature is already discussed in the earlier paper [26] to show linear dependency in view of Γ vs E_U plot, the other phonon modes are also examined here in a similar way as described for $EuFeO_3$. The significance of the present study is that it elaborates analytically on the strength of combined optical and Raman spectroscopy techniques to perceive the disorder sensitivity of a phonon mode, which can help understand the the lattice dynamics in perturbed systems, potentially useful in understanding the phonon-specific transport properties of materials.

II. EXPERIMENTAL METHODS

The polycrystalline bulk $EuFeO_3$ (EFO) sample was prepared via wet chemical synthesis (sol-gel method), and the polycrystalline TiO_2 sample was procured. Moreover, the *in situ* optical absorption spectra of the samples were recorded with the help of a UV-Vis spectrophotometer [40,55,56] attached with an in-house developed temperature varying assembly [57]. The TD Raman spectra were recorded with the help of a high-resolution Raman spectrometer in backscattering mode equipped with 633 nm excitation laser and charge-coupled detector [58–60]; the temperature controller stage was used to vary the sample temperature [61]. The details on sample preparation, characterization, and TD spectra of EFO are provided elsewhere [49].

III. ANALYTICAL BACKGROUND

The empirical relation [Eq. (5)] bridges the physical quantities Γ and E_U through the parameter ξ [26,49,50], which come from two different spectroscopic techniques, namely Raman (Γ) and optical spectroscopies (E_U). Clearly, ξ imparts the change in Γ of a phonon mode when the E_U (total disorder) in the system changes owing to the perturbation, thus, the name disorder sensitivity. Even though the previous studies indicate a constant ξ because of linear Γ vs E_U plots in the considered range of perturbing parameter (doping % vs chemical disorder, and temperature vs thermal disorder) [26,49,50], it is interesting to ask the nature of ξ in overall range. The well-adopted models on temperature variation of Γ and E_U can help investigate the temperature dependence of ξ, and therefore, the thermal disorder as the lattice perturbation is emphasized in the present paper. Another motivation to examine the temperature dependence of ξ is that the E_U extends from few meV to hundreds of meV [62–64], being the similar range of the phonon spectra. Then, ξ may also contain the information of the interaction of electrons in the disorder band ($\sim E_U$) with the nearby phonons (Γ), and this interaction would have finite dependence on the temperature; so should ξ. It should be noted that for a disorder free system

$$E_U \to 0, \quad \text{but } \Gamma \neq 0, \tag{6}$$

which is taken care by the parameter λ in the empirical relation Eq. (5). Hence, one can write

$$as \;\; E_U \to 0, \quad \Gamma \to \lambda. \tag{7}$$

Thus, λ appears to be a real, positive, and disorder-independent parameter that possibly contains information of the intrinsic phonon linewidth in absence of any disorder. Nevertheless, no system, in practice, is disorder free even at absolute zero; therefore, practically, $\Gamma(0K) > \lambda$ can be expected. For a linear Γ vs E_U plot, the intercept can give the parameter λ, and there may lie following possibilities of its values: $\lambda \leqslant 0, \lambda \geqslant 0$ or $\lambda = 0$; $\lambda > 0$ makes more sense whose physical meaning would be that as $E_U \to 0$, $\Gamma \to \lambda$. The cases $\lambda < 0$ and/or $\lambda = 0$ suggest that as the system acquires minimal disorder, i.e., $E_U \to 0$, $\Gamma < 0$ and/or $\Gamma = 0$, respectively, which is practically not plausible. Nevertheless, there can be two interpretations to this: first, any negative values of λ for a given system can be inferred that it is not feasible for that system to reach disorder free state; and second, the Γ vs E_U curve may deviate from its linear behavior in certain temperature range in order to hold the fundamental nature of the two quantities as per the physics aspect. This is where the quest for main investigation starts. As ξ can be seen as the slope of the Γ vs E_U plot (which may or may not be linear in all ranges), we can simply visualize it as

$$\xi = \frac{d\Gamma}{dE_U}. \tag{8a}$$

For understanding the influence of thermal disorder, we consider the temperature dependent case

$$\xi(T) = \left(\frac{d\Gamma(T)}{dT}\right)\left(\frac{dE_U(T)}{dT}\right)^{-1}. \tag{8b}$$

The E_U and Γ are both known to increase systematically with sample temperature [41,43,46], which can be understood as increase in the density of states (DOS) of Urbach tail because of enhanced spread in the electronic states near the band edges [41,65], and likewise, the phonon lifetimes alter because of the anharmonicity, resulting in the increasing Γ with temperature [23,46], The symmetric broadening of phonon modes can attribute to the phonon-phonon interactions, and while analyzing such Raman modes, the peaks can be fitted with Lorentzian function. However, in a case of an energetic overlap of discrete phonon with the electronic continuum states, i.e., coupling of the phonons with electrons near band edges there can occur finite probability of Fano resonance [26,60,66]. Thus, the presence of disorder may add finite probability to the system to exhibit electron-phonon interactions, contributing to the asymmetric broadening of the respective phonon mode depending upon the overlapped electronic—and phononic—DOS, thus, modifies the line shape. Therefore, the analysis of such phonon modes with finite asymmetry can be carried out with Fano function [26,66]: $I(\omega) = A \cdot \frac{(q+\epsilon)^2}{1+\epsilon^2} + B$; $\epsilon = \frac{\omega-\omega_0}{\Gamma/2}$ where A and B are scaling factors, q is the asymmetry parameter whose magnitude is inversely related to the asymmetry of the lineprofile, ω_0 is related to the peak position, and Γ is the peak width. Furthermore, having the ingredients to initiate this analytical investigation on $\xi = \xi(T)$ in the form of the $\Gamma(T)$ and $E_U(T)$ models, we start it with considering the case of 3ph process and thus finding $\xi(T)_{3ph}$. Differentiating the expression for $\Gamma(T)_{3-ph}$ [Eq. (3)] and E_U [Eq. (2)], we get

$$\left.\frac{d\Gamma(T)}{dT}\right|_{3-ph} = \frac{\Gamma_0\hbar\omega_0}{k_B}\frac{1}{T^2}\frac{\exp(\hbar\omega_0/2k_BT)}{(\exp(\hbar\omega_0/2k_BT)-1)^2}, \tag{9}$$

$$\frac{dE_U(T)}{dT} = E_{02}\Theta_E\frac{1}{T^2}\frac{\exp(\Theta_E/T)}{(\exp(\Theta_E/T)-1)^2}. \tag{10}$$

Thereby, proceeding in accordance with Eq. (8), we have

$$\begin{aligned}\Rightarrow \xi(T)|_{3-ph} &= \frac{d\Gamma/dT|_{3-ph}}{dE_U/dT} \\ &= \frac{\Gamma_0\hbar\omega_0}{E_{02}k_B\Theta_E}\frac{\exp(\hbar\omega_0/2k_BT)}{\exp(\Theta_E/T)} \\ &\quad\times\frac{(\exp(\Theta_E/T)-1)^2}{(\exp(\hbar\omega_0/2k_BT)-1)^2}.\end{aligned} \tag{11}$$

Moreover, as discussed in Sec. I about the importance of including contribution owing to four-phonon process, similar steps for the same gives the following:

$$\begin{aligned}\left.\frac{d\Gamma(T)}{dT}\right|_{4-ph} &= \frac{\hbar\omega_0\Gamma_{01}}{T^2}\frac{\exp(\hbar\omega_0/2k_BT)}{(\exp(\hbar\omega_0/2k_BT)-1)^2} \\ &\quad+\frac{\hbar\omega_0\Gamma_{02}}{T^2}\left(\frac{\exp(\hbar\omega_0/3k_BT)}{(\exp(\hbar\omega_0/3k_BT)-1)^2}\right. \\ &\quad\left.+\frac{2\exp(\hbar\omega_0/3k_BT)}{(\exp(\hbar\omega_0/3k_BT)-1)^3}\right),\end{aligned} \tag{12}$$

which further gives

$$\xi(T)|_{4-ph} = \frac{\hbar\omega_0}{k_B\Theta_E E_{02}}\left(\Gamma_{01}\frac{e^{\hbar\omega_0/2k_BT}}{e^{\Theta_E/T}}\left(\frac{e^{\Theta_E/T}-1}{e^{\hbar\omega_0/2k_BT}-1}\right)^2 + \Gamma_{02}\frac{e^{\hbar\omega_0/3k_BT}}{e^{\Theta_E/T}}\left(\left(\frac{e^{\Theta_E/T}-1}{e^{\hbar\omega_0/3k_BT}-1}\right)^2 + 2\frac{(e^{\Theta_E/T}-1)^2}{(e^{\hbar\omega_0/3k_BT}-1)^3}\right)\right). \quad (13)$$

Usually, the Raman shifts in the light frequency are expressed in wavenumber units $\bar{\nu}$ (cm^{-1}). In that case, ω_0 (in angular frequency units) can be expressed as $\omega_0 \sim 2\pi c\bar{\nu}_0$; $c \rightarrow$ cm/s, and $\bar{\nu}_0$ cm^{-1}. With that consideration, the symbols $\omega \longleftrightarrow \bar{\nu}$ are interchangeably used in the present text and all the shifts will be put in the equations after multiplication with c that takes care of the dimensionality ($\hbar\omega = hc\bar{\nu}$ in energy units). Moreover, Γ_0, Γ_{01}, Γ_{02} are readily put as such in the wavenumber units (cm^{-1}), which ultimately gives the ξ in cm^{-1}/meV. This is the same unit of the ξ appearing in the empirical relation [Eq. (5)], and can be helpful to understand the phonon properties conveniently. It is clear from Eqs. (11) and (13) that the term $\xi(T)$ depends on the Einstein temperature (Θ_E) as well as the intrinsic mode frequency (ω_0), which indicates its phonon-mode specific behavior. Also, the appearance of additional terms in the expression of $\xi(T)_{4-ph}$ suggests some deviation than $\xi(T)_{3-ph}$ in extended temperature ranges that will be investigated further.

IV. EXPERIMENTAL INVESTIGATION ON $\xi(T)$

A. Temperature dependence of $\xi(T)$

In order to experimentally explore the temperature dependence of the parameter ξ, the experimental data for E_U and Γ are considered for the two different systems: $EuFeO_3$ and TiO_2, one being a multiferroic perovskite oxide and other being a well-explored semiconductor, respectively. Importantly, polycrystalline materials often exhibit features such as grain boundaries, point defects, dislocations, microstrain, and so forth [67–69], which can significantly enhance the E_U and Γ. The scattering processes in the material will be altered because of the presence of these features, that can further enhance with sample temperature, leading to stronger sensitivity of phonons. In addition, the coupling of phonons with electrons can indeed play a role in influencing the sensitivity of the phonons [49,70,71]. Therefore, observation of a greater change in Γ with increase in E_U for a polycrystalline sample is anticipated that can possibly make the experimental probing of temperature dependence of ξ more conveniently realizable. Thus, the samples are chosen in polycrystalline form. For the case when E_U is small, the electrons in the well-defined states near the band edge can significantly participate in the coupling with phonons, which can be expected to take place at much lower temperatures. However, at higher temperatures, the well-defined states may undergo smearing and manifest into the the Urbach band. Indeed, the nature of these electronic states will be distinct, and thus, the electron-phonon contribution into the overall behavior of sensitivity of phonons can vary in different temperature regions. Because of finite

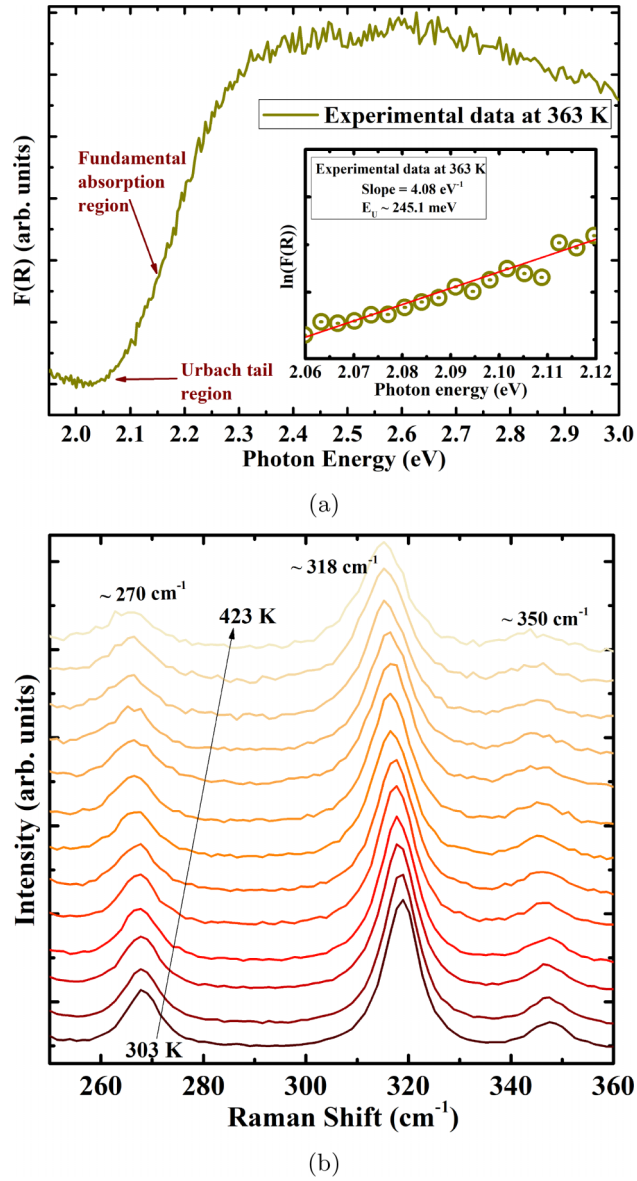

FIG. 1. Schematic representation of (a) optical absorption spectra collected at 363 K, $F(R)$ is Kubelka Munk function, being proportional to the absorption coefficient. The inset represents fitting of the $\ln(F(R))$ in the Urbach tail region in accordance with Urbach rule to find the E_U; (b) Raman spectra of the EFO sample collected at different sample temperatures. The detailed description on Urbach rule, Raman analysis, and related steps can be found elsewhere [36,49].

overlapping between energy span of electronic band and the phonons, typically in meV range, there occurs finite probability for the phonons to interact with the Urbach electrons, which indeed reflects as a consequence of the disorder in the system affecting the coupling. In that view, the collected optical absorption and Raman spectra are shown in Fig. 1, and the $E_U(T)$ extracted from the recorded diffuse reflectance spectra for EFO sample is shown in the Fig. 2, fitted with Einstein oscillator model Eq. (2). Clearly, the E_U can be seen to systematically increase with temperature attributing to the increase in the disorder within the system.

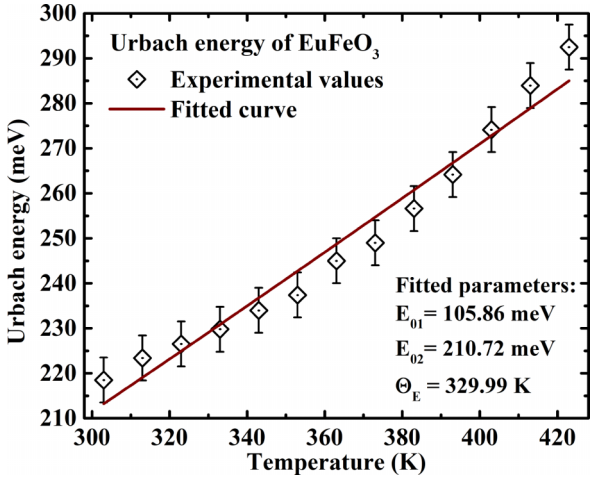

FIG. 2. Plot of temperature variation of Urbach energy in $EuFeO_3$. Experimental data points fitted with Einstein oscillator model.

In orthoferrites like systems, the valence band (VB) is mostly contributed by the *O*–2*p* orbitals whereas the conduction band (CB) is dominated by the *Fe*–3*d* orbitals [72]. Furthermore, it is known that the contribution of Urbach tail states is greater near the VB [40,73], the phonon modes associated with the vibrations of respective ions can be of interest for the current investigation. Also, phonon modes being nondegenerate (single identifiable) are usually suitable, and can be fitted to extract linewidths. $EuFeO_3$ stabilizes in space group *Pnma* with 24 Raman-active modes [74], but only a few of these modes of interest are readily resolved to satisfactorily perform fitting in order to have the information of necessary parameters. Therefore, the temperature variation of few of the Raman modes in range 250–350 cm^{-1} has been chosen in current investigation; the modes in this range associate with the Fe-O vibrations.

The TD Raman spectra of the prepared EFO sample have been collected in the range ∼303–423 K and the evolution of the extracted peak position [$\omega(T)$] and width [$\Gamma(T)$] for the ∼318 cm^{-1} mode are depicted in Fig. 3; these have been fitted with the *three-phonon* [Fig. 3(a)] and *four-phonon* models [Fig. 3(b)]. Also, in order to have the information of ω_0, the temperature-dependent Raman shift data was fitted with the Balkanski model [21] by using following relations for (i) three-phonon process:

$$\omega(T) = \omega_0 + A\left(1 + \frac{2}{\exp(\hbar\omega_0/2k_BT) - 1}\right) \tag{14}$$

and for (ii) four-phonon phonon process

$$\omega(T) = \omega_0 + A\left(1 + \frac{2}{\exp\left(\frac{\hbar\omega_0}{2k_BT}\right) - 1}\right) + B\left(1 + \frac{3}{\exp\left(\frac{\hbar\omega_0}{3k_BT}\right) - 1} + \frac{3}{\left(\exp\left(\frac{\hbar\omega_0}{3k_BT}\right) - 1\right)^2}\right). \tag{15}$$

Thus, the required parameters in Eqs. (11) and (13) can be obtained in order to simulate the ξ_{3ph} and ξ_{4ph}. It is noteworthy in the present case that the investigation concerns with the temperature variation in Raman linewidth ($\frac{d\Gamma}{dT}$) rather than precise determination of its absolute constant value at a temperature, thereby rendering the effect of instrumental broadening insignificant; hence, the contribution of instrumental broadening to the final results can be overlooked without concern. Furthermore, the Γ vs E_U plot is also obtained in Fig. 4. For examining the trend of experimentally observed quantities in the extended temperature ranges, the simulated linewidth and the Urbach energy are drawn via the fitting parameters of related plots; using these, theoretical Γ vs E_U curves have been generated for 3ph and 4ph processes, which is compared with the corresponding experimental plot (Fig. 4). The experimental data has been considered for linear fit [Eq. (5)] giving

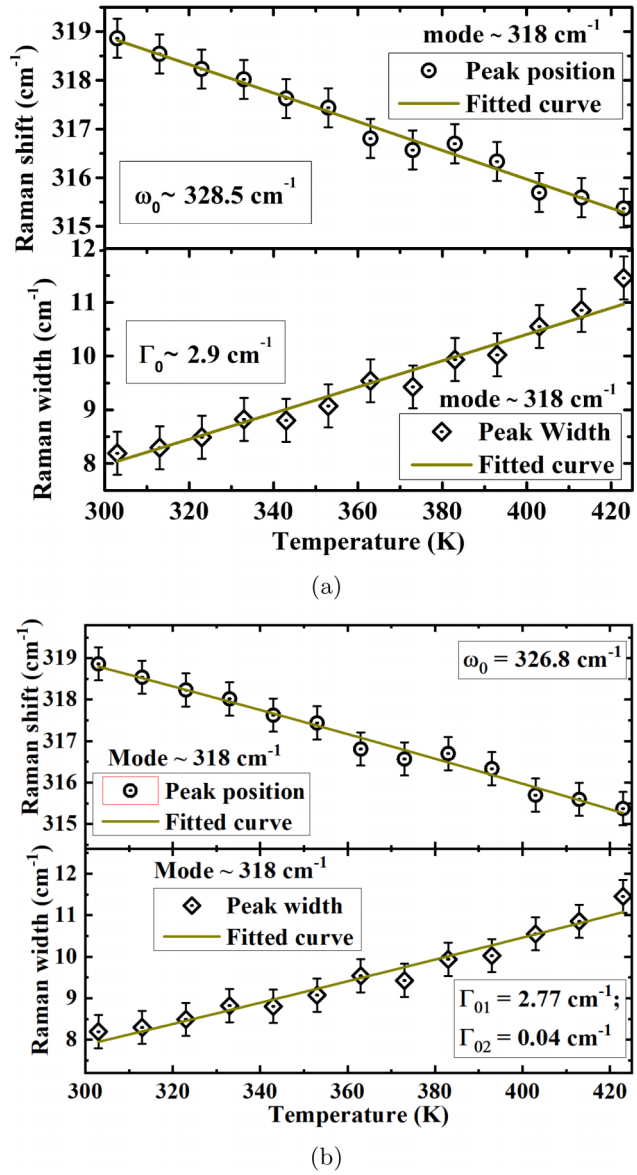

FIG. 3. Schematic representation of the temperature variation of the peak position and Raman linewidth of ∼318 cm^{-1} mode in bulk $EuFeO_3$ fitted with (a) three-phonon process model to find the values of ω_0 and Γ_0; and those fitted with (b) Balkanski four-phonon model to find the values of ω_0 and Γ_{01}, Γ_{02}.

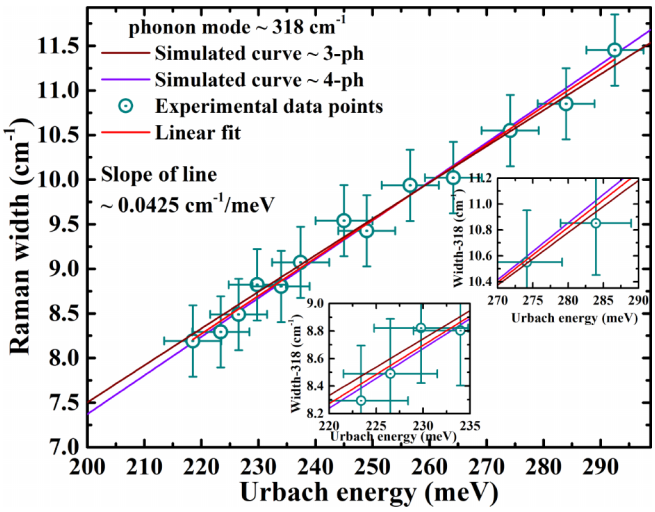

FIG. 4. Plot of Raman linewidth of 318 cm^{-1} mode vs Urbach energy in bulk $EuFeO_3$. Data points following the linear behavior along the line fit (red) compared with the simulated trace (violet 4-phonon process, brown 3-phonon process).

a slope value of 0.0425 cm^{-1}/meV, which is also consistent with the values obtained for this phonon mode in the earlier report [49]. The simulated curves appear within the error bars of the data points and are quite linear even away from the data points, emphasizing that the slope of the Γ vs E_U curve varies little so that the quantity Γ seems to exhibit linear behavior with respect to increase in E_U, or constant appearing value of ξ, even though the derived expressions suggested finite temperature dependence. This can be precisely analyzed by explicitly considering the variation of $\xi(T)$.

Now, having values of all the parameters required to be put in Eqs. (11) and (13), the theoretical realization of $\xi(T)$ can be made. The simulated curve has been drawn in Fig. 5

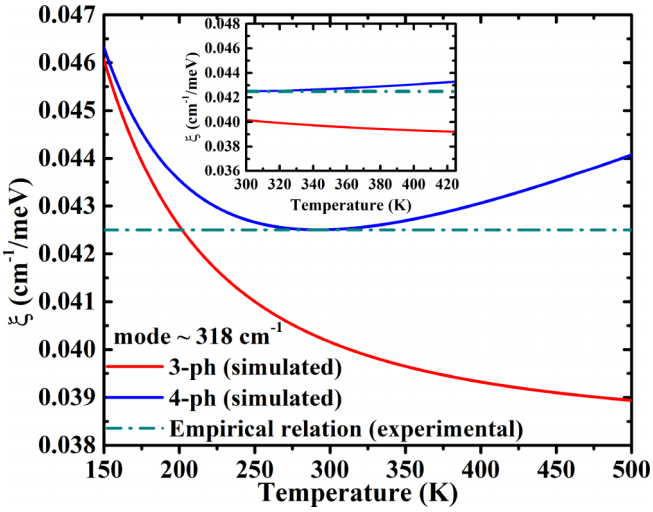

FIG. 5. Plot of temperature variation of parameter ξ showing the comparison of theoretically simulated behavior (for 3ph and for 4ph) with the experimentally observed value. Inset shows the same output in the temperature region of experimental observation. The curve for ξ_{4-ph} lies closer to the spectroscopically observed value.

for the phonon mode ~318 cm^{-1}. The theoretically obtained trend advocates the temperature dependence of ξ, even though slow at higher temperatures, whose significance is that the change of Raman linewidth for a phonon mode with respect to the change in total disorder in the system (E_U) is not at all constant in the entire temperature range. At low temperatures, both the simulated curves for 3ph and 4ph processes go along. However, it is interesting to see that at higher temperatures, the evolution of $\xi(T)$ exhibits a strong dependence on the considered scattering process. The curve simulated for 3ph process [$\xi(T)_{3-ph}$] significantly diverges from that for $\xi(T)_{4-ph}$ and varies asymptotically, attaining a value far from the experimentally observed slope (i.e., empirically obtained ξ) depicted as a dashed line corresponding to linear fit of the $\Gamma(T)$ vs E_U data in accordance with Eq. (5).

In addition, an inset is also provided within the Fig. 5 whose temperature range is confined to the temperature range of experimental measurements. It shows that even though the parameter ξ exhibits temperature dependence, it evolves gradually in the temperature range of the experiment, which should be the main reason of the constant-appearing slope or the linear behavior of Γ vs E_U plot. Further, it is noteworthy from the inset that $\xi(T)_{4-ph}$ lies closer to the value obtained from the linear fit in contrast to $\xi(T)_{3-ph}$. This could be further interpreted as the importance of four phonon process over three phonon process in the lattice dynamics of the considered system, i.e., EFO sample.

The similar simulations are also generated for the Raman modes ~270 and ~350 cm^{-1} of EFO, and reveal the similar interpretations of $\xi(T)$. The related figures are provided in the Appendix A.

B. Interpretation of the derived behavior of $\xi(T)$

In order to understand the derived behavior of ξ in more general sense, a systematic examination of its dependence on temperature as well as the Einstein temperature (Θ_E) is now performed by means of simulations; the compiled results of these simulations are presented in video files within the Supplemental Material [75] and a simpler depiction is provided in Fig. 6. These simulations have been generated from the derived expressions for ξ_{3ph} [Eq. (11)] and ξ_{4ph} [Eq. (13)], which gave an interesting output. In Fig. 6(a), the $\xi_{3-ph}(T)$ variation for $\Theta_E = 303$ K is depicted in the sbubfigure (i) and the correlated E_U vs $\Gamma(T)$ plot is drawn in subfigure (ii); the same for $\xi_{4-ph}(T)$ is also depicted in subfigures (iii) and (iv). Since the E_U and $\Gamma(T)$ are the direct physical observables in this case, the expected change in the respective E_U vs $\Gamma(T)$ plots is depicted within the temperature region closely related to the experimentally accessible range in the current study along with a linear reference line drawn for comparison by eye. Similar aspects are also presented in Fig. 6(b) for the case of a material with higher Θ_E (~ 808 K). Clearly, a deviation from the linear behavior can be realized at greater Θ_E, i.e., for materials with higher Θ_E. The simulation not only revealed the temperature dependence of ξ [i.e., $\xi(T)$] but also indicates that higher the Θ_E greater would be $\xi(T)$, which will be feasible for experimental realization of the temperature dependence of $\xi(T)$. A clearer depiction can be realized in the compiled animation video of these simulated figures, which

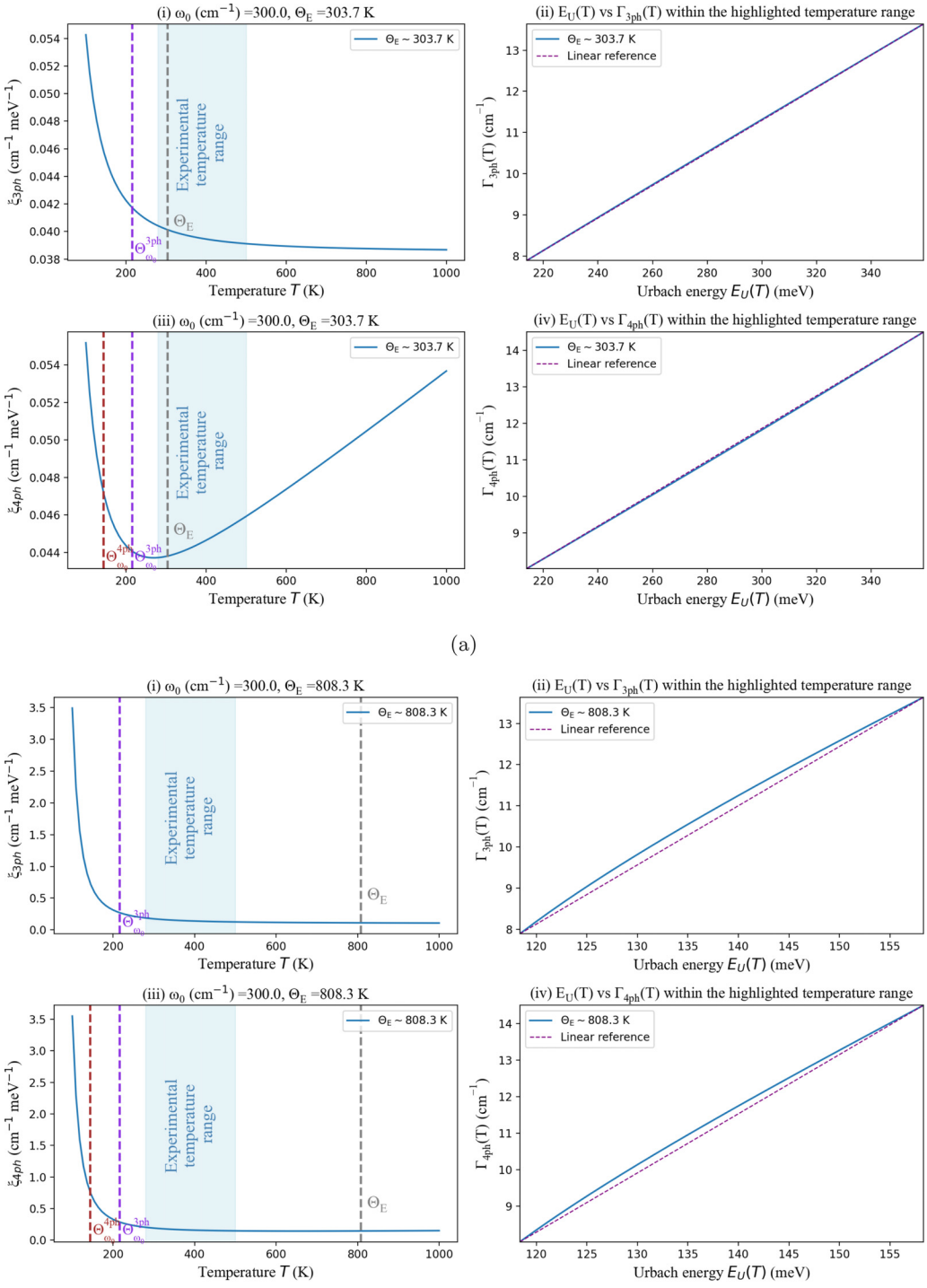

FIG. 6. Simulated $\xi(T)$ for 3ph and 4ph processes for a phonon mode in a material with different Θ_E. (a) 303 K and (b) 808 K. The respective subfigures (ii) and (iv) depict expected E_U vs $\Gamma(T)$ in the highlighted temperature regions in (i) and (iii).

are provided as files I and II within the Supplemental Material [75]. The file I represents the dependence in form of a 2D contour plot for the same, which visualizes the $\xi(T, \Theta_E)$, and the file II is same depiction in form of a 2D $\xi(T)$ plot at different Θ_E values for precisely presenting the comparison of E_U vs Γ plot. In connection with this Supplemental Material and the Fig. 6, we discuss the following:

Considering the subfigure (i) of the Fig. 6(a), it can be realized that the ξ_{3ph} exhibits a monotonically decreasing trend with temperature, in contrast to the case of ξ_{4ph}

[subfigure (iii)] where the ξ seems to increase beyond certain temperature. A careful analysis suggests that the relative separation between phonon temperature $\Theta_{\omega_0}^{3ph}$ $(= \hbar\omega_0/2k_B)$ and the Θ_E play important role in determining this point. In this case, both $\Theta_{\omega_0}^{3ph}$ and Θ_E are closer. In contrast, the subfigure (iii) of same figure exhibits a reversal-like behavior in $\xi_{4ph}(T)$ plot appearing near $T \sim \Theta_{\omega_0}^{4ph}$ when $\Theta_E > \Theta_{\omega_0}^{3ph}$, where the phonon temperature $\Theta_{\omega_0}^{4ph} = \hbar\omega_0/3k_B$. However, since the sensitivity has smaller magnitude, it can be said that its temperature dependence does not satisfactorily reflect in the direct observation of the E_U vs $\Gamma(T)$ with the material of lower Θ_E [Figs. 6(a)(ii) and 6(a)(iv)], explaining the linear trend.

In spite of that, for the case of higher Θ_E [Fig. 6(b)], the trend of both ξ_{3ph} and ξ_{4ph} seems to acquire similar monotonically decreasing behavior with temperature. Nevertheless, the magnitude of simulated ξ appears to be sufficient enough that even the slight variation with temperature can reflect in the E_U vs $\Gamma(T)$ plot [Figs. 6(b)(ii) and 6(b)(iv)]. Thus, it can be interesting to extending the experimental investigation to a material with higher Θ_E and realizing the temperature dependence of ξ via direct observation of the E_U vs $\Gamma(T)$ plot deviating from linear behavior as seen in the simulation. In that view, TiO_2 sample has been of interest as its Θ_E is well above the room temperature, which has been discussed in next section.

V. EXTENSION OF THE APPROACH ON TiO_2 SYSTEM

The representatives for collected data for the *in situ* TD optical absorption spectra and *in situ* TD Raman spectra of the TiO_2 sample are provided in Fig. 7; the corresponding temperature variation of the extracted $E_U(T)$ and $\Gamma(T)$ for a phonon mode ($\sim$395 cm^{-1}) are shown in Figs. 8(a) and 8(b), respectively, which clearly show a monotonous increment attributing to enhanced scattering processes within the sample with temperature and, hence, reduced phonon lifetime that reflects as the broadened peaks [22,30]. Now, following the similar steps as in the case of EFO sample, the plot of Γ vs E_U is obtained for the Raman modes of the sample and is depicted in the Fig. 9(a) for $\sim$395 cm^{-1} mode. The simulated curves for this plot are also drawn by using the parameters shown in Fig. 8 for the 3-phonon and 4-phonon processes. In addition, as per the empirical relation Eq. (5), the linear fit is also drawn over the presented values, which gives a slope value of $\sim$0.2 cm^{-1}/meV, which is significantly higher than that observed for the phonon modes of EFO sample being even $<$0.1 cm^{-1}/meV. Consequently, the dynamic behavior of the slope of Γ vs E_U plot can be realized as its deviation from the linear trend. In particular, the plot can be seen to bend along positive x axis, which is also followed by the simulated curves for both 3- and 4-phonon process. It suggests that as the E_U increases, the slope (rate of change of linewidth with respect to E_U) decreases, or slows, emphasizing the temperature dependence of ξ. This is further confirmed by

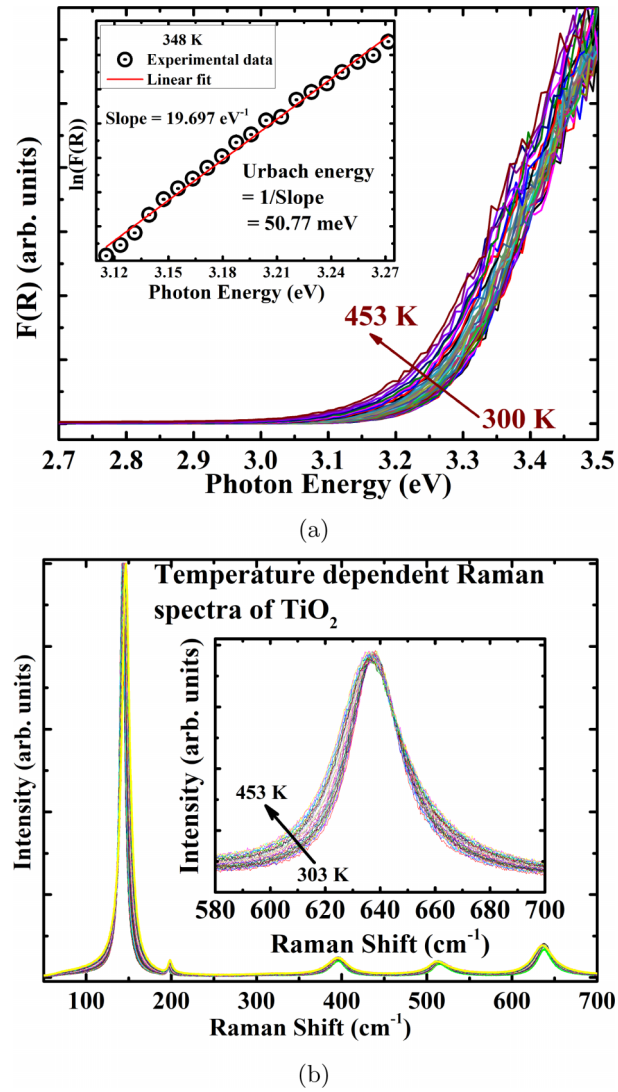

FIG. 7. Schematic representation of temperature-dependent (a) optical absorption spectra collected in diffuse reflectance mode, F(R) is Kubelka Munk function, being proportional to the absorption coefficient; and (b) Raman spectra of polycrystalline TiO_2 sample.

drawing another simulation for $\xi(T)$ [Fig. 9(b)] obtained by using the parameters listed in Fig. 8 into the Eqs. (11) and (13). Clearly, the observed trend is in alignment with the inferences drawn in this discussion, i.e., ξ decreases monotonically with temperature for both kinds of phonon processes, as was discussed for the materials with high Θ_E with the simulation example of Fig. 6(b). The inset of figure shows the same in the experimental temperature range, which shows that the slope value ξ lies far enough at lower temperatures from the linear-apparent slope value ($\sim$0.236 cm^{-1}/meV) and drops closer at higher temperature where the variation becomes relatively gradual. The noticeable divergence between the linear

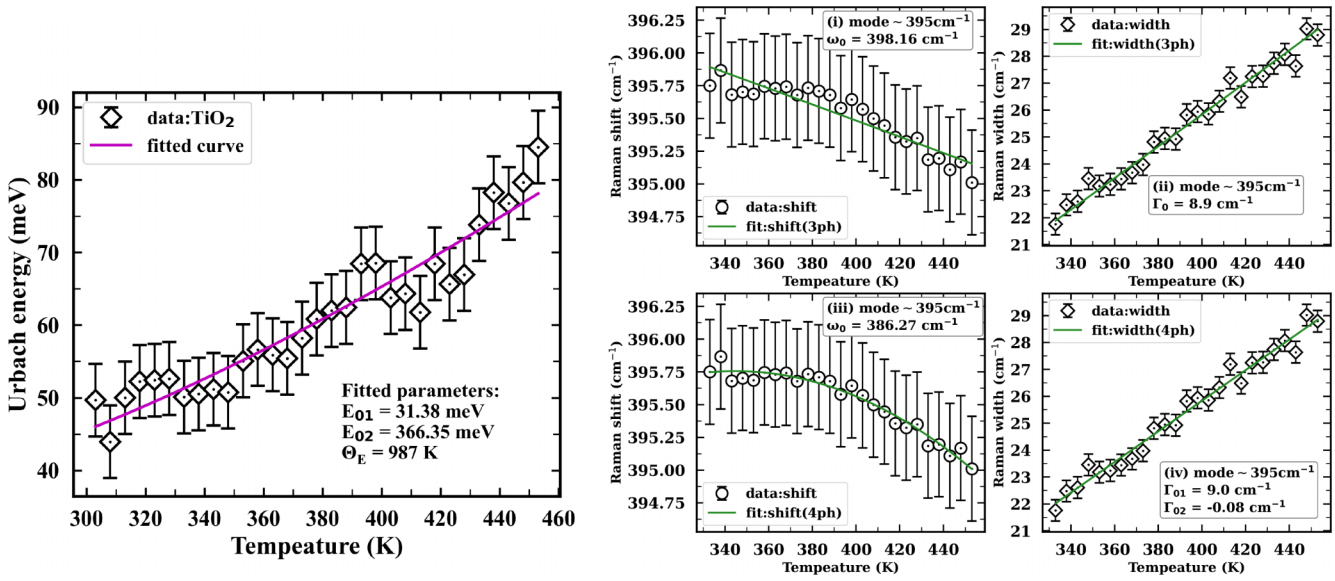

(a) (b)

FIG. 8. (a) Schematic representation of temperature variation of the extracted Urbach energy showing increment with temperature in polycrystalline TiO_2 sample. (b) Representative plots of temperature variation of Raman shifts and linewidths for the Raman mode ~395 cm^{-1}. Shift, width, respectively, fitted with 3-phonon model in (i) and (ii), and 4-phonon model in (iii) and (iv).

fit and the simulated Γ vs E_U curves at lower E_U values for TiO2 sample Fig. 9(a) supports the discussed model of ξ. On comparing this with the Γ vs E_U plot for the EFO sample (Fig. 4), the ξ for EFO is low enough that the simulated curves do not deviate much from the linear fit despite the temperature dependence of ξ. The trend is best explained by the

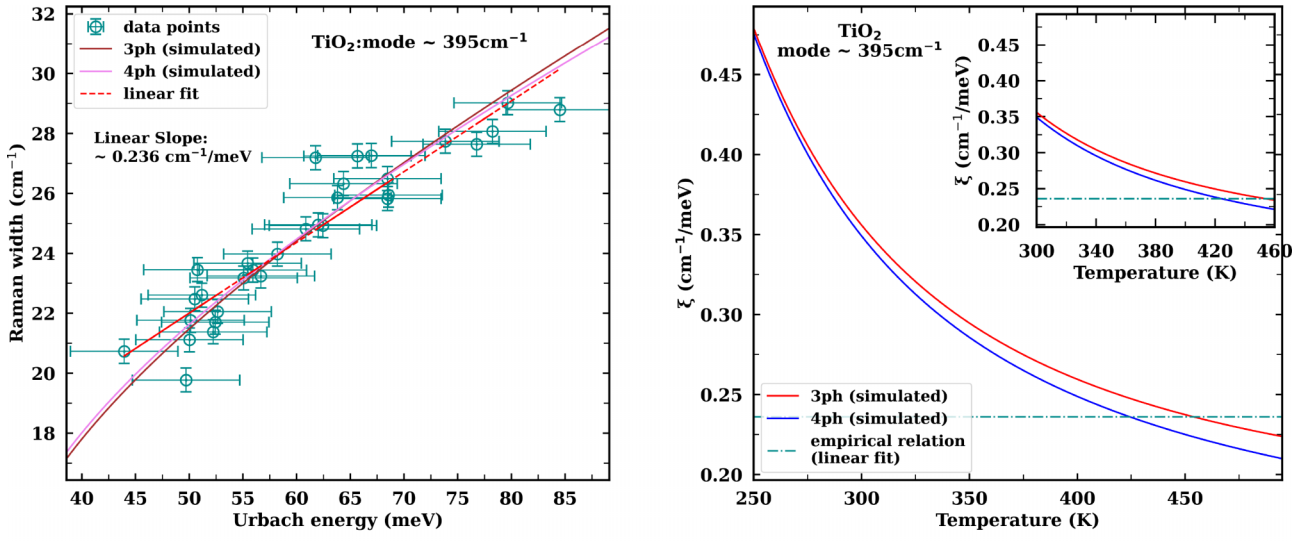

(a) (b)

FIG. 9. (a) Schematic for $\Gamma(T)$ vs $E_U(T)$ plots for ~395 cm^{-1} Raman mode of the TiO_2 sample, represented with the simulated curves. A deviation from linear fit is visible, attributing to the temperature dependence of the slope, i.e., ξ. (b) Simulated plot for ξ using the derived relations for 3- and 4-phonon processes.

contribution of 4-phonon process (Fig. 5) because of which the $\xi(T)$ does not monotonically decrease and the linearity of the Γ vs E_U plot gets compensated, which is not the case for TiO_2 owing to its high Θ_E value than EFO.

Moreover, the similar can also be realized on the other phonon modes in TiO_2, and the related schematics are shown in Appendix B (phonon modes $640\,cm^{-1}$, $196\,cm^{-1}$, and $140\,cm^{-1}$). Interestingly, it can be realized from these plots that the slope of Γ vs E_U curve for the phonon modes of TiO_2 sample progressively varies with temperature, which signifies the temperature-dependent nature of the quantity ξ, the disorder sensitivity of the phonon modes. It also signifies that the temperature variation of ξ is realized in the wide-range plot. Furthermore, looking at the trends of Γ vs E_U plots of both of the physical systems, namely, EFO and TiO_2, it can be interpreted that the evolution of $\xi(T)$ is not only governed by the thermal parameter Θ_E but also by the dynamic coefficient of Urbach energy as can be seen from the comparison of $E_U(T)$ plots of the samples. It implies that as a system acquires (thermal) disorder, the disorder sensitivity of phonon modes would exhibit considerable changes in the considered wide temperature range where the evolution of the total disorder $E_U(T)$ is rapid. In the case of TiO_2, the Θ_E is above room temperature [41,53] in contrast to the case of orthoferrites where it is comparatively close to the room temperature [54]. In the single oscillator picture, since the Θ_E corresponds to the temperature at/above which the thermal perturbation may excite a quantum harmonic oscillator; therefore, a significant variation in the disorder sensitivity of a vibrational mode should be visible when the Θ_E is above the room temperature, which has also been observed in the simulation. However, the variation in ξ may not be much visible in the otherwise case, i.e., $T \sim \Theta_E$ or $T > \Theta_E$, because the population would have been already excited and not much change could be measurable in minute temperature range. Nevertheless, it will also be important to consider the coefficient of dynamic part of the Urbach energy [Eq. (2)] as it can be understood to contain the information of the evolution of the disorder, which can be a factor affecting the ground-state population. This explains the Γ vs E_U trend experimentally observed for both TiO_2 and $EuFeO_3$ systems. The study of the slope ξ for different phonons can be of importance while considering the phonon transport properties within a system as it can affect the physical properties [11,76–78].

VI. CONCLUSIONS

In this study, we investigated the temperature-dependent behavior of the disorder sensitivity (ξ) of phonon modes, defined as the rate of change of the Raman linewidth (Γ) with respect to the Urbach energy (E_U). Using both theoretical models [the Balkanski model for $\Gamma(T)$ and the Einstein oscillator model for $E_U(T)$] and experimental data from polycrystalline $EuFeO_3$ and TiO_2, we observed a gradual temperature dependence of ξ over a wide thermal range. Near and above room temperature, ξ exhibits a pseudoconstant nature, explaining the observed linear relationship between Γ and E_U.

This paper demonstrates that while the temperature evolution of ξ is finite, the relative separation between Einstein temperature (Θ_E) and the phonon temperature ($\Theta^{3ph}_{\omega_0} \sim \hbar\omega_0/2k$) plays an important role in determining the sensitivity, such that both the magnitude and temperature dependence of ξ were found stronger for $\Theta_E > \Theta^{3ph}_{\omega_0}$. The findings offer fundamental insights into lattice dynamics, particularly in terms of the role of disorder in influencing phonon lifetimes. Moreover, the study highlights the potential of using simultaneous analysis of Raman linewidth and Urbach energy to identify specific phonons for selective excitation. Such an approach can be useful for controlling transport properties in strongly correlated systems, where phonon-resolved disorder sensitivity plays a critical role. By consolidating these findings, we provide a comprehensive understanding of the relationship between phonon linewidth and Urbach energy, i.e., the quantities related to phonons and electrons, respectively, in terms of disorder sensitivity, with potential implications for material design and tuning of thermal properties in semiconductor and dielectric systems.

ACKNOWLEDGMENTS

Sophisticated Instrumentation Center, IITI is acknowledged for some of the characterization facilities. O.V.R. acknowledges IIT Indore and the Ministry of Education, Govt. of India, for financial support through Teaching Assistantship. K.K. acknowledges CSIR New Delhi for providing financial assistance through NET-JRF Grant No. 1121851885. Department of Science and Technology, Fund for Improvement of S&T Infrastructure (SR/FST/PSI-225/2016) is acknowledged for funding the Raman spectrometer. P.R.S. and O.V.R. acknowledge IIT Indore for providing financial support. Dr. Er. Nitin Upadhyay, Dept. of Physics, IITI, is sincerely acknowledged for his technical assistance in Raman measurements. Authors acknowledge Dr. Sudeep Tiwari for fruitful discussions. Dr. Anil Kumar is thanked for his valuable feedback. Aarti Lakhara and Mohit Choubisa are thanked for their helpful insights.

O.V.R. conceptualized the scientific problem, wrote manuscript, synthesised $EuFeO_3$, performed experimental measurements—Raman and diffuse reflectance spectroscopies, simulation, data analysis (theory and experiment). K.K. contributed to scientific discussions, assisted in experiments and analysis. P.R.S. contributed to scientific discussions, manuscript editing, guidance, and supervision of the scientific work.

Authors declare no conflicts of interest.

APPENDIX A: SCHEMATICS FOR OTHER PHONON MODES IN $EuFeO_3$

1. Phonon mode ~270 cm^{-1}

The similar analysis is extended to the phonon mode near 270 cm^{-1} (extraction of parameters required for simulation is depicted in Fig. 10). The experimental data points for Γ vs E_U plot seem to follow a linear trend which can also be realized by the simulated curves for both 3ph and 4ph process [Fig. 11(a)]. However, the simulated $\xi(T)$ for this mode [Fig. 11(b)] reveals that the slope varies gradually in the experimental temperature range (inset), and the 4ph process dominate as the curve traces closer to the observed slope value obtained via fitting the pseudo linear behavior.

2. Phonon mode ~350 cm^{-1}

Another demonstration is provided for the phonon mode near 350 cm^{-1} (extraction of parameters required for simulation is depicted in Fig. 12). Similar to the other two modes, data points for Γ vs E_U plot exhibit a linear trend [Fig. 13(a)]. However, the simulated $\xi(T)$ [Fig. 13(b)] reveals the variation of slope in the experimental temperature range (inset).

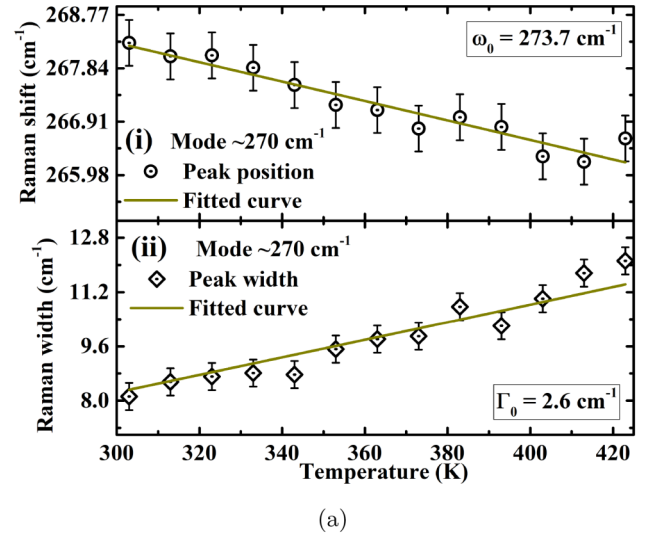

(a)

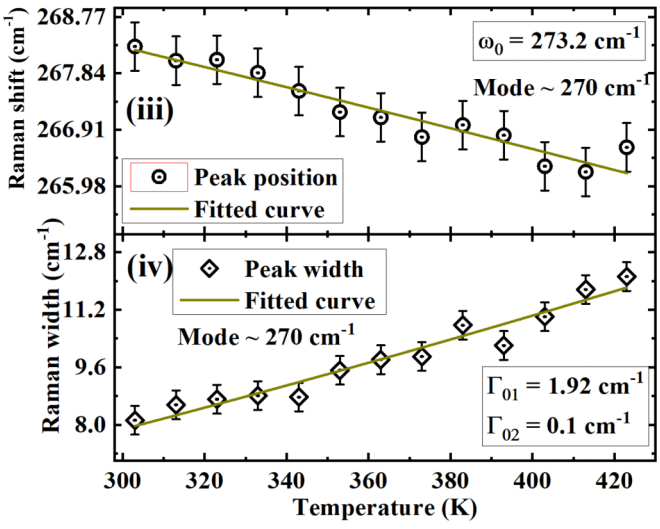

(b)

FIG. 10. Representation of the temperature variation of peak position and Raman linewidth of ~270 cm^{-1} mode in bulk $EuFeO_3$ fitted with three-phonon process (3ph) model [(a)(i) and (a)(ii)] to find the values of ω_0 and Γ_0; and fitted with Balkanski four-phonon (4ph) model [(b)(iii) and (b)(iv)] to find the values of ω_0 and Γ_{01}, Γ_{02}.

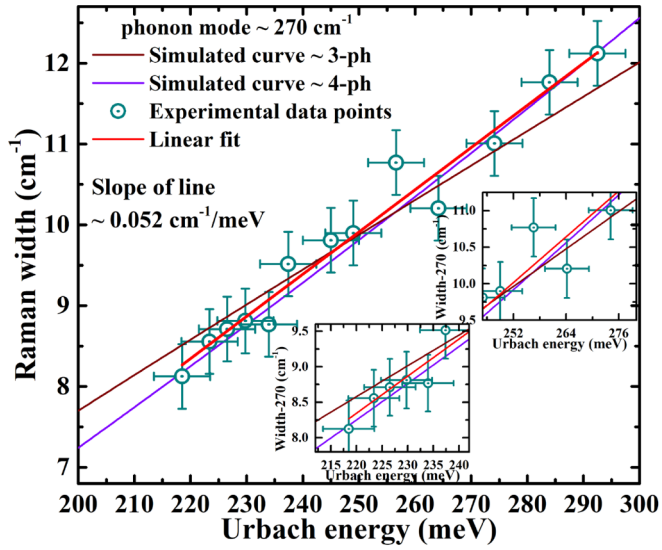

(a)

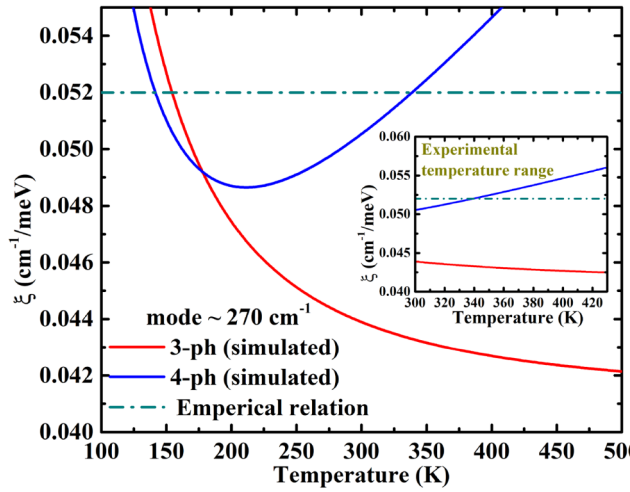

(b)

FIG. 11. (a) Plot of Γ(T) of 270 cm^{-1} mode vs E_U in bulk $EuFeO_3$. The line fit (red) is compared with the simulated trace (violet 4-phonon process, brown 3-phonon process). (b) Temperature variation of parameter ξ showing the comparison of theoretically simulated behavior (for 3ph and 4ph processes) with the ξ obtained empirically. Inset shows the same output in the experimental temperature range.

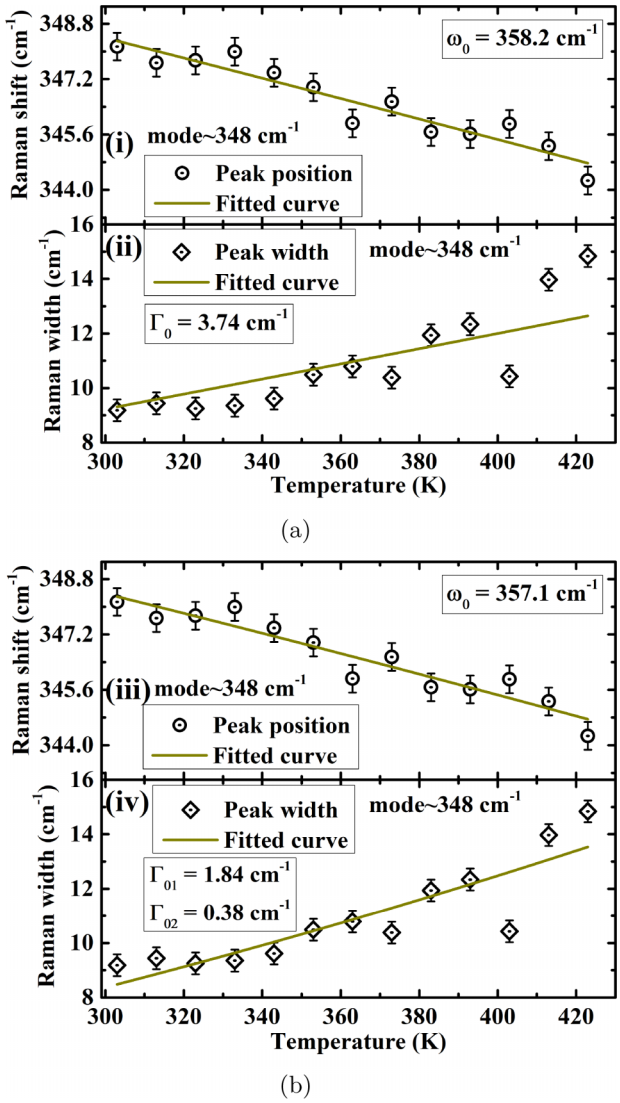

FIG. 12. Schematic representation of the temperature variation of the peak position and Raman linewidth of ~348 cm^{-1} mode in bulk $EuFeO_3$ fitted with three-phonon process model [(a)(i) and (a)(ii)] to find the values of ω_0 and Γ_0; and those fitted with Balkanski four-phonon model [(b)(iii) and (b)(iv)] to find the values of ω_0 and Γ_{01}, Γ_{02}.

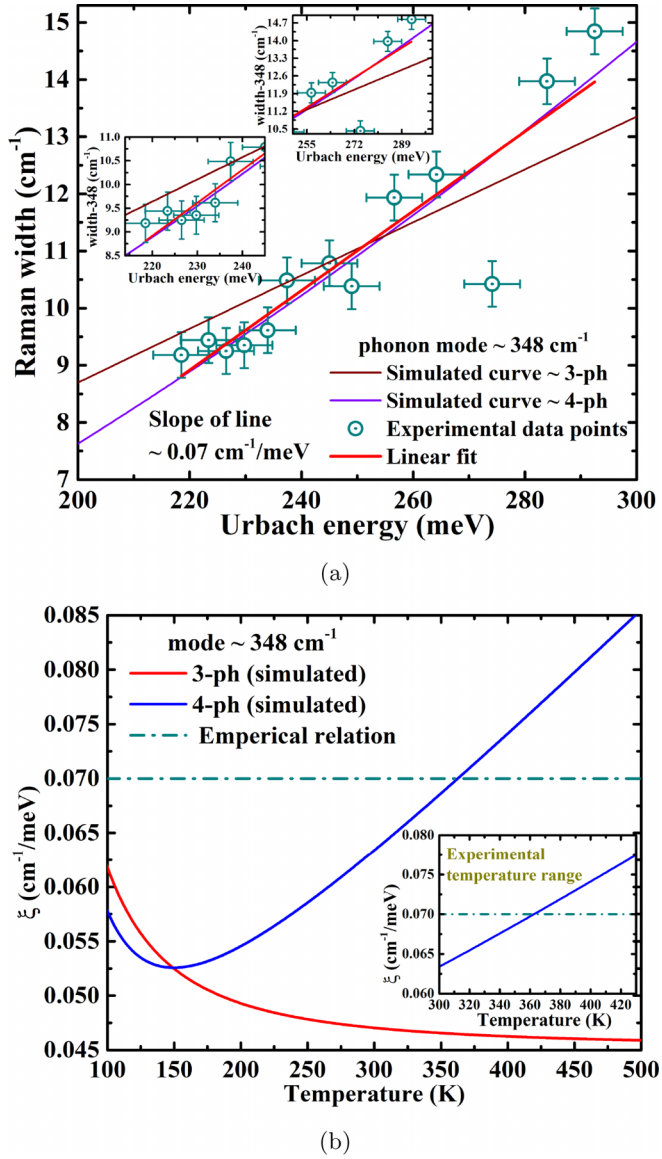

FIG. 13. (a) Plot of Raman linewidth of 348 cm^{-1} mode vs Urbach energy in bulk $EuFeO_3$. Data points following the linear behavior along the line fit (red) compared with the simulated trace (violet 4-phonon process, brown 3-phonon process). (b) Temperature variation ξ showing the comparison of theoretically simulated behavior (for 3ph and 4ph processes) with the ξ observed empirically. Inset shows the same output in the experimental temperature range.

APPENDIX B: SCHEMATICS FOR OTHER PHONON MODES IN TiO_2

1. Phonon mode ~640 cm^{-1}

In contrast to the case of EFO, TiO_2 is found to exhibit greater ξ values for its modes, which helps visualizing the temperature variation of $\xi(T)$ itself as a finite deviation of Γ vs E_U data points can be seen. Figure 14 depicts the extraction of Raman parameters needed for the simulation. Figure 15 demonstrates the same for the phonon mode near 640 cm^{-1}. The simulated $\xi(T)$ Fig. 16 also reveals monotonically decreasing behavior with temperature that explains the deviation of data points from the linear trend.

2. Phonon mode ~196 cm^{-1}

Another demonstration of the temperature dependence of the sensitivity $\xi(T)$ is shown for phonon mode near 196 cm^{-1} (Raman parameters extracted from the fit are shown in Fig. 17), which can be realized as the deviation of Γ vs E_U data points from linearity Fig. 18. The simulated curve for this plot satisfactorily follows the data points and the simulated $\xi(T)$ Fig. 19 also reveals monotonically decreasing behavior explaining the trend.

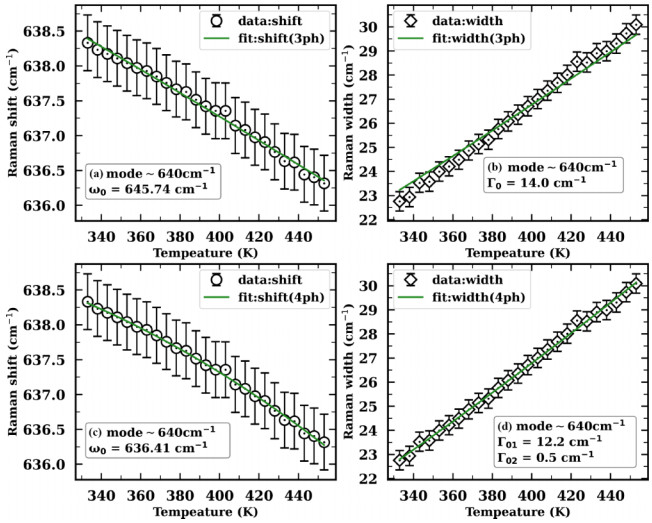

FIG. 14. Schematic representation of the temperature variation of Raman shift, linewidth fitted with 3-phonon model in (a) and (b) , and 4-phonon model in (c) and (d), respectively, for ∼640 cm^{-1} phonon mode of TiO_2 sample. The extracted parameters to be used for simulations are listed within the plots.

3. Phonon mode ∼140 cm^{-1}

An additional demonstration for phonon mode near 140 cm^{-1} is shown with necessary Raman parameters extracted from the fit shown in Fig. 20), which further confirms the deviation of Γ vs E_U data points from linearity Fig. 21.

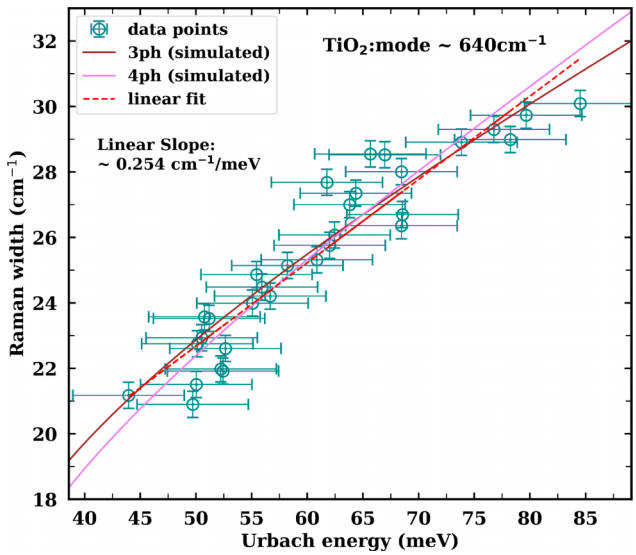

FIG. 15. Representative of Γ vs E_U plot with experimental data points and the simulated curves for both 3-phonon (brown) and 4-phonon (violet) processes for ∼640 cm^{-1} phonon mode of TiO_2. The linear fit is shown with dashed red line.

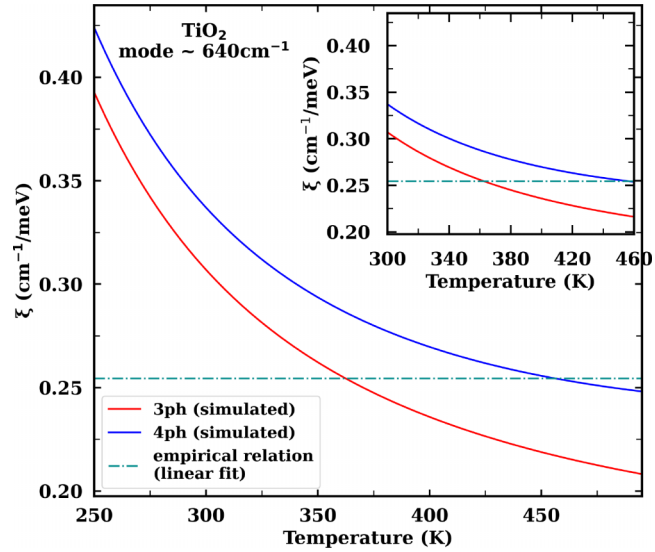

FIG. 16. Simulated plot for ξ for ∼640 cm^{-1} phonon mode in TiO_2 using the derived relations for 3- and 4-phonon processes. The slope obtained from linear fit is shown as dash-dot line.

The simulated curves for this plot also satisfactorily follow the data points and the simulated $\xi(T)$ Fig. 22 reveals monotonically decreasing behavior explaining the trend. This is in alignment with the theoretically inferred influence of high Θ_E on the sensitivity $\xi(T)$.

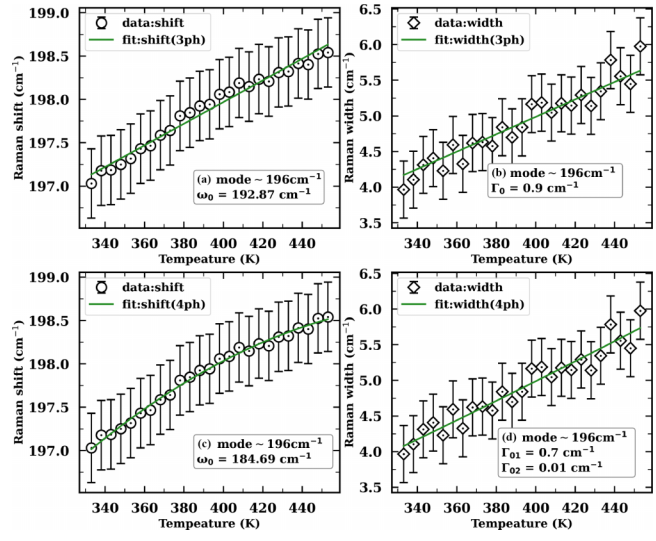

FIG. 17. Schematic representation of the temperature variation of Raman shift, linewidth fitted with 3-phonon model in (a) and (b), and 4-phonon model in (c) and (d), respectively, for ∼196 cm^{-1} phonon mode of TiO_2 sample. The extracted parameters to be used for simulations are listed within the plots.

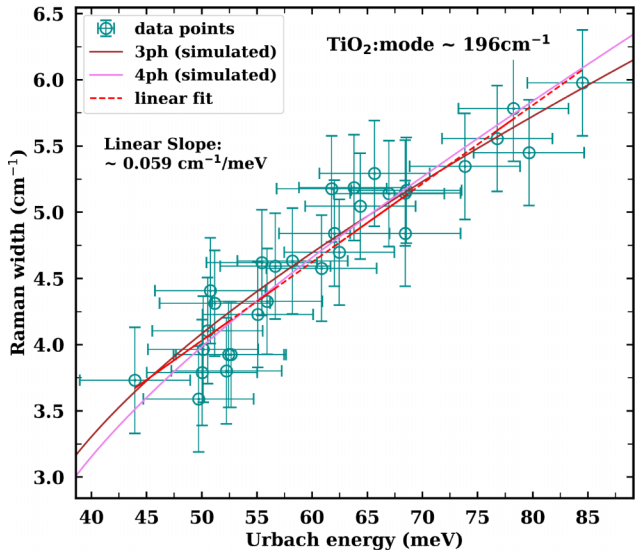

FIG. 18. Representative of Γ vs E_U plot with experimental data points and the simulated curves for both 3-phonon (brown) and 4-phonon (violet) processes for ∼196 cm^{-1} phonon mode of TiO_2. The linear fit is shown with dashed red line.

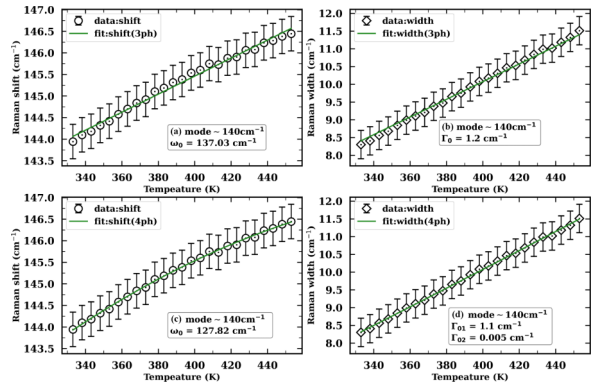

FIG. 20. Schematic representation of the temperature variation of Raman shift, linewidth fitted with 3-phonon model in (a) and (b), and 4-phonon model in (c) and (d), respectively, for ∼140 cm^{-1} phonon mode of TiO_2 sample. The extracted parameters to be used for simulations are listed within the plots.

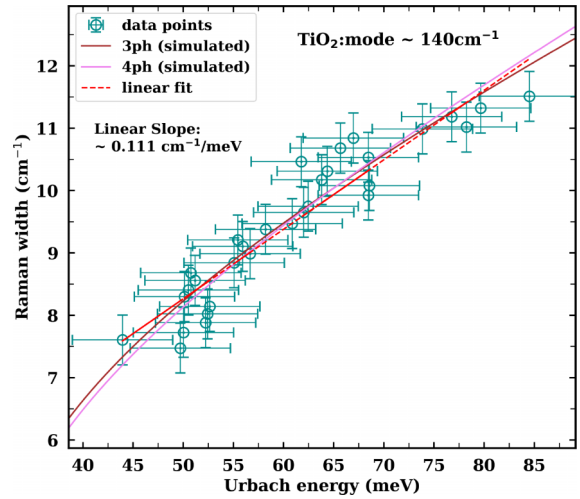

FIG. 21. Representative of Γ vs E_U plot with experimental data points and the simulated curves for both 3-phonon (brown) and 4-phonon (violet) processes for ∼146 cm^{-1} phonon mode of TiO_2. The linear fit is shown with dashed red line.

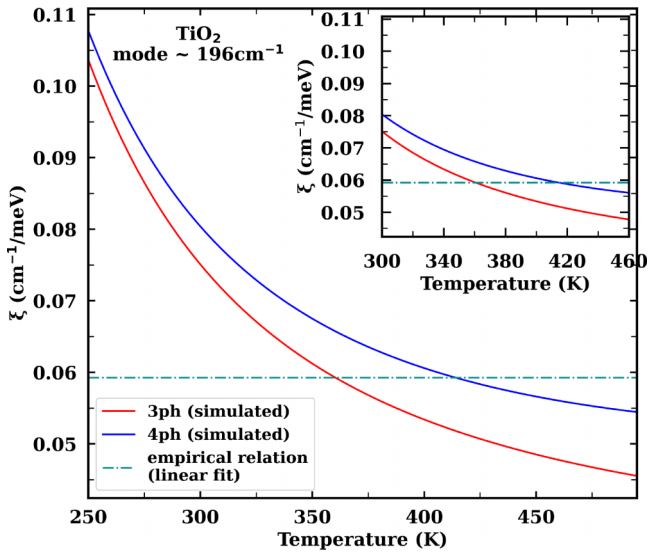

FIG. 19. Simulated plot for ξ for ∼196 cm^{-1} phonon mode in TiO_2 using the derived relations for 3- and 4-phonon processes. The slope obtained from linear fit is shown as dash-dot line.

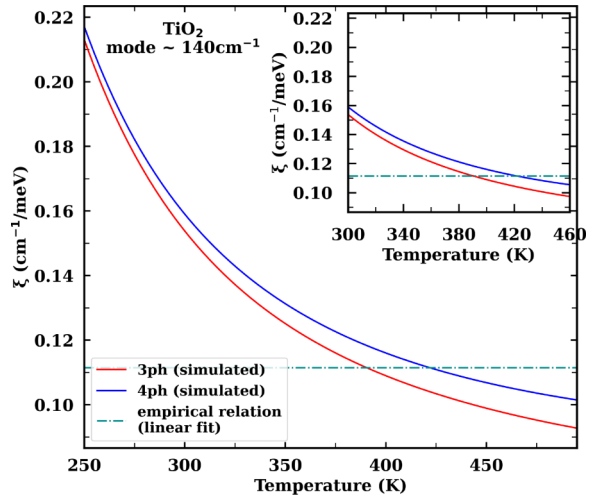

FIG. 22. Simulated plot for ξ for ∼140 cm^{-1} phonon mode in TiO_2 using the derived relations for 3- and 4- phonon processes. The slope obtained from linear fit is shown as dash-dot line.

[1] D. Samanta, A. Mazumder, S. P. Chaudhary, B. Ghosh, P. Saha, S. Bhattacharyya, and G. D. Mukherjee, Phonon anharmonicity and soft-phonon mediated structural phase transition in $Cs_3Bi_2Br_9$, Phys. Rev. B **108**, 054104 (2023).

[2] F. Formalik, M. Fischer, and B. Kuchta, Correlating phonons and deformations: A method for structural phase transformation analysis in metal–organic frameworks, Cryst. Growth Des. **23**, 8962 (2023).

[3] A. I. Krivchikov, A. Jeżowski, D. Szewczyk, O. A. Korolyuk, O. O. Romantsova, L. M. Buravtseva, C. Cazorla, and J. L. Tamarit, Role of optical phonons and anharmonicity in the appearance of the heat capacity boson peak-like anomaly in fully ordered molecular crystals, J. Phys. Chem. Lett. **13**, 5061 (2022).

[4] J. Bhosale, A. K. Ramdas, A. Burger, A. Muñoz, A. H. Romero, M. Cardona, R. Lauck, and R. K. Kremer, Temperature dependence of band gaps in semiconductors: Electron-phonon interaction, Phys. Rev. B **86**, 195208 (2012).

[5] R. Saran, A. Heuer-Jungemann, A. G. Kanaras, and R. J. Curry, Giant bandgap renormalization and exciton–phonon scattering in perovskite nanocrystals, Adv. Opt. Mater. **5**, 1700231 (2017).

[6] A. Sapkota, Y. Li, B. L. Winn, A. Podlesnyak, G. Xu, Z. Xu, K. Ran, T. Chen, J. Sun, J. Wen, L. Wu, J. Yang, Q. Li, G. D. Gu, and J. M. Tranquada, Electron-phonon coupling and superconductivity in the doped topological crystalline insulator $(Pb_{0.5}Sn_{0.5})_{1-x}In_xTe$, Phys. Rev. B **102**, 104511 (2020).

[7] H. Anzai, M. Arita, H. Namatame, M. Taniguchi, M. Ishikado, K. Fujita, S. Ishida, S. Uchida, and A. Ino, A new landscape of multiple dispersion kinks in a high-T_c cuprate superconductor, Sci. Rep. **7**, 4830 (2017).

[8] K. Yoshida, T. Sonobe, H. Zen, K. Hachiya, K. Okumura, K. Mishima, M. Inukai, H. Negm, K. Torgasin, M. Omer, T. Kii, K. Masuda, and H. Ohgaki, Experimental demonstration of mode-selective phonon excitation of 6H-SiC by a mid-infrared laser with anti-Stokes Raman scattering spectroscopy, Appl. Phys. Lett. **103**, 182103 (2013).

[9] I. Yu. Sklyadneva, G. Benedek, E. V. Chulkov, P. M. Echenique, R. Heid, K.-P. Bohnen, and J. P. Toennies, Mode-selected electron-phonon coupling in superconducting Pb nanofilms determined from He atom scattering, Phys. Rev. Lett. **107**, 095502 (2011).

[10] S. Kaiser, Light-induced superconductivity in high-Tc cuprates, Phys. Scr. **92**, 103001 (2017).

[11] A. Ungeheuer, A. S. Hassanien, M. T. Mir, L. Nöding, T. Baumert, and A. Senftleben, Selective excitation of higher harmonic coherent acoustic phonons in a graphite nanofilm, J. Phys. Chem. C **126**, 19822 (2022).

[12] O. Sato, K. Yoshida, H. Zen, K. Hachiya, T. Goto, T. Sagawa, and H. Ohgaki, Two-photon selective excitation of phonon-mode in diamond using mid-infrared free-electron laser, Phys. Lett. A **384**, 126223 (2020).

[13] C. H. Grein and S. John, Temperature dependence of the Urbach optical absorption edge: A theory of multiple phonon absorption and emission sidebands, Phys. Rev. B **39**, 1140 (1989).

[14] S. Sahoo, A. P. S. Gaur, M. Ahmadi, M. J.-F. Guinel, and R. S. Katiyar, Temperature-dependent Raman studies and thermal conductivity of few-layer MoS_2, J. Phys. Chem. C **117**, 9042 (2013).

[15] F. Yue, J. W. Tomm, D. Kruschke, B. Ullrich, and J. Chu, Temperature dependence of the fundamental excitonic resonance in lead-salt quantum dots, Appl. Phys. Lett. **107**, 022106 (2015).

[16] M. Gupta, S. C. Shirbhate, O. V. Rambadey, S. A. Acharya, and P. R. Sagdeo, Temperature-dependent delocalization of oxygen vacancies in La-substituted CeO_2, ACS Appl. Energy Mater. **5**, 9759 (2022).

[17] G. E. Franklin, E. Fontes, Y. Qian, M. J. Bedzyk, J. A. Golovchenko, and J. R. Patel, Thermal vibration amplitudes and structure of As on Si(001), Phys. Rev. B **50**, 7483 (1994).

[18] E. J. Baran, Mean amplitudes of vibration of the halogen molecules, Z. Natur. A **58**, 36 (2003).

[19] K. W. Böer and U. W. Pohl, Phonon-induced thermal properties, in *Semiconductor Physics* (Springer International Publishing, Cham, 2014) pp. 1–25.

[20] X. Yang, J. Tiwari, and T. Feng, Reduced anharmonic phonon scattering cross-section slows the decrease of thermal conductivity with temperature, Mater. Today Phys. **24**, 100689 (2022).

[21] M. Balkanski, R. F. Wallis, and E. Haro, Anharmonic effects in light scattering due to optical phonons in silicon, Phys. Rev. B **28**, 1928 (1983).

[22] O. V. Rambadey, M. Gupta, A. Kumar, and P. R. Sagdeo, Analysis of structural disorder on Raman spectra of semiconductors, J. Appl. Phys. **133**, 131101 (2023).

[23] T. R. Hart, R. L. Aggarwal, and B. Lax, Temperature dependence of Raman scattering in silicon, Phys. Rev. B **1**, 638 (1970).

[24] T. Ohsaka, Temperature dependence of the Raman spectrum in anatase TiO_2, J. Phys. Soc. Jpn. **48**, 1661 (1980).

[25] A. Kumar, V. Mishra, M. K. Warshi, A. Sati, A. Sagdeo, R. Kumar, and P. R. Sagdeo, Strain induced disordered phonon modes in Cr doped $PrFeO_3$, J. Phys.: Condens. Matter **31**, 275602 (2019).

[26] O. V. Rambadey, A. Kumar, and P. R. Sagdeo, Investigating the correlation between the Urbach energy and asymmetry parameter of the Raman mode in semiconductors, Phys. Rev. B **104**, 245205 (2021).

[27] M. D. Joshi, N. K. Kumbhar, O. V. Rambadey, P. R. Sagdeo, R. S. Devan, and S. S. Hosmani, Exfoliated nano-hBN additives for enhancing tribological performance of ATSP coatings deposited on AISI 316L steel: Role of SMAT pre-treatment, Surf. Coat. Technol. **447**, 128829 (2022).

[28] A. Sunny, A. Thirumurugan, and K. Balasubramanian, Laser induced Fano scattering, electron–phonon coupling, bond length and phonon lifetime changes in α-Fe_2O_3 nanostructures, Phys. Chem. Chem. Phys. **22**, 2001 (2020).

[29] A. Kumar, M. K. Warshi, V. Mishra, S. K. Saxena, R. Kumar, and P. R. Sagdeo, Strain control of Urbach energy in Cr-doped $PrFeO_3$, Appl. Phys. A **123**, 576 (2017).

[30] P. Mishra, M. Tangi, T. K. Ng, M. N. Hedhili, D. H. Anjum, M. S. Alias, C.-C. Tseng, L.-J. Li, and B. S. Ooi, Impact of N-plasma and Ga-irradiation on MoS_2 layer in molecular beam epitaxy, Appl. Phys. Lett. **110**, 012101 (2017).

[31] M. Gupta, O. V. Rambadey, A. Sagdeo, and P. R. Sagdeo, Investigating the structural, vibrational, optical, and dielectric properties in Mg-substituted $LaAlO_3$, J. Mater. Sci.: Mater. Electron. **33**, 13352 (2022).

[32] A. Sati, V. Mishra, A. Kumar, M. Warshi, A. Sagdeo, R. Kumar, and P. Sagdeo, Effect of structural disorder on the electronic and

phononic properties of Hf doped $BaTiO_3$, J. Mater. Sci.: Mater. Electron. **30**, 9498 (2019).
[33] M. Gupta, A. Kumar, A. Sagdeo, and P. R. Sagdeo, Doping-induced combined Fano and phonon confinement effect in La-doped CeO_2: Raman spectroscopy analysis, J. Phys. Chem. C **125**, 2648 (2021).
[34] A. Iribarren, R. Castro-Rodríguez, V. Sosa, and J. L. Peña, Modeling of the disorder contribution to the band-tail parameter in semiconductor materials, Phys. Rev. B **60**, 4758 (1999).
[35] M. V. Kurik, Urbach rule, Phys. Stat. Sol. (a) **8**, 9 (1971).
[36] O. V. Rambadey, A. Kumar, A. Sati, and P. R. Sagdeo, Exploring the interrelation between Urbach energy and dielectric constant in Hf-substituted $BaTiO_3$, ACS Omega **6**, 32231 (2021).
[37] A. Kumar, M. K. Warshi, V. Mishra, A. Sati, S. Banik, A. Sagdeo, R. Kumar, and P. Sagdeo, Optical spectroscopy: An effective tool to probe the origin of dielectric loss in Cr doped $PrFeO_3$, Ceramics Int. **45**, 8585 (2019).
[38] I. Studenyak, M. Kranjec, and M. Kurik, Urbach rule in solid state physics, Optics **4**, 76 (2014).
[39] J. A. Guerra, L. Montañez, F. De Zela, A. Winnacker, and R. Weingärtner, On the origin of the Urbach rule and the Urbach focus, MRS Proc. **1536**, 139 (2013).
[40] A. Kumar, O. V. Rambadey, and P. R. Sagdeo, Unorthodox approach to realize the correlation between the dielectric constant and electronic disorder in Cr-doped $PrFeO_3$, J. Phys. Chem. C **125**, 7378 (2021).
[41] V. Mishra, M. K. Warshi, A. Sati, A. Kumar, V. Mishra, R. Kumar, and P. R. Sagdeo, Investigation of temperature-dependent optical properties of TiO_2 using diffuse reflectance spectroscopy, SN Appl. Sci. **1**, 241 (2019).
[42] N. Mokdad, F. Z. Mami, N. Boukli-Hacène, K. Zitouni, and A. Kadri, Theoretical study of Urbach tail behavior in $Hg_{1-x}Cd_xTe$ in the $0.21 \leqslant x \leqslant 0.6$ medium and far infrared optical ranges, J. Appl. Phys. **132**, 175702 (2022).
[43] M. Ledinsky, T. Schönfeldová, J. Holovský, E. Aydin, Z. Hájková, L. Landová, N. Neyková, A. Fejfar, and S. De Wolf, Temperature dependence of the Urbach energy in lead iodide perovskites, J. Phys. Chem. Lett. **10**, 1368 (2019).
[44] J. Chantana, Y. Kawano, T. Nishimura, A. Mavlonov, and T. Minemoto, Impact of Urbach energy on open-circuit voltage deficit of thin-film solar cells, Sol. Energy Mater. Sol. Cells **210**, 110502 (2020).
[45] M. Bhowmick, H. Xi, and B. Ullrich, Optical bandgap definition via a modified form of Urbach's rule, Materials **14**, 1639 (2021).
[46] J. LaCombe and J. Irwin, The temperature dependence of the optical phonon linewidths and frequencies in ZnSe and ZnTe, Solid State Commun. **8**, 1427 (1970).
[47] S. Gopalan, P. Lautenschlager, and M. Cardona, Temperature dependence of the shifts and broadenings of the critical points in GaAs, Phys. Rev. B **35**, 5577 (1987).
[48] J. Huso, H. Che, D. Thapa, A. Canul, M. D. McCluskey, and L. Bergman, Phonon dynamics and Urbach energy studies of MgZnO alloys, J. Appl. Phys. **117**, 125702 (2015).
[49] O. V. Rambadey, A. Kumar, K. Kumar, V. Mishra, and P. R. Sagdeo, Methodology to probe disorder contribution in Raman linewidth via optical absorption spectroscopy in orthoferrite $EuFeO_3$, J. Phys. Chem. C **126**, 13946 (2022).
[50] K. Kumar, O. V. Rambadey, and P. R. Sagdeo, Deconvolution of phonon–phonon and electron–phonon interactions from phonon line width in Zr-substituted $BaTiO_3$, J. Phys. Chem. C **127**, 22164 (2023).
[51] R. Cowley, Raman scattering from crystals of the diamond structure, J. Phys. France **26**, 659 (1965).
[52] S. R. Johnson and T. Tiedje, Temperature dependence of the Urbach edge in GaAs, J. Appl. Phys. **78**, 5609 (1995).
[53] S. J. Smith, R. Stevens, S. Liu, G. Li, A. Navrotsky, J. Boerio-Goates, and B. F. Woodfield, Heat capacities and thermodynamic functions of TiO_2 anatase and rutile: Analysis of phase stability, Am. Mineral. **94**, 236 (2009).
[54] A. Scrimshire, A. Lobera, A. M. T. Bell, A. H. Jones, I. Sterianou, S. D. Forder, and P. A. Bingham, Determination of Debye temperatures and Lamb–Mössbauer factors for $LnFeO_3$ orthoferrite perovskites (Ln = La, Nd, Sm, Eu, Gd), J. Phys.: Condens. Matter **30**, 105704 (2018).
[55] O. V. Rambadey, M. Gupta, and P. R. Sagdeo, Phonon-mode-specific lattice dynamical coupling of carriers in semiconductors using Raman and optical spectroscopic techniques, Phys. Rev. B **106**, 075204 (2022).
[56] K. Kumar, O. V. Rambadey, and P. R. Sagdeo, Contribution of individual phonon to the band gap renormalization in semiconductors, Phys. Scr. **99**, 075932 (2024).
[57] V. Mishra, M. Warshi, R. Kumar, and P. Sagdeo, Design and development of *in-situ* temperature dependent diffuse reflectance spectroscopy setup, J. Inst. **13**, T11003 (2018).
[58] A. Kumar, O. V. Rambadey, H. Rai, and P. R. Sagdeo, Role of laser excitation wavelength and power in the Fano resonance scattering in $RFe_{0.50}Cr_{0.50}O_3$ (R = Sm, Er, and Eu): A brief Raman study, J. Phys. Chem. C **126**, 5403 (2022).
[59] M. Gupta, O. V. Rambadey, and P. R. Sagdeo, Probing the effect of R-cation radii on structural, vibrational, optical, and dielectric properties of rare earth (R = La, Pr, Nd) aluminates, Ceramics Int. **48**, 23072 (2022).
[60] O. V. Rambadey, K. Kumar, R. Nain, A. Kumar, P. R. Sagdeo, P. M. Chamberlin, and K. W. Adu, Shedding light on evolution of Raman line shape with probing laser power: Light-induced perturbation in electron–phonon coupling, J. Chem. Phys. **161**, 034202 (2024).
[61] A. Kumar, M. K. Warshi, A. Sagdeo, M. Krzystyniak, S. Rudić, D. T. Adroja, I. da Silva, and P. R. Sagdeo, Origin of natural and magnetic field induced polar order in orthorhombic $PrFe_{1/2}Cr_{1/2}O_3$, Phys. Rev. B **104**, 035101 (2021).
[62] J. Chantana, T. Nishimura, Y. Kawano, S. Teraji, T. Watanabe, and T. Minemoto, Examination of relationship between Urbach energy and open-circuit voltage deficit of flexible $Cu(In, Ga)Se_2$ solar cell for its improved photovoltaic performance, ACS Appl. Energy Mater. **2**, 7843 (2019).
[63] E. Ugur, M. Ledinský, T. G. Allen, J. Holovský, A. Vlk, and S. De Wolf, Life on the Urbach edge, J. Phys. Chem. Lett. **13**, 7702 (2022).
[64] I. Bonalde, E. Medina, M. Rodríguez, S. M. Wasim, G. Marín, C. Rincón, A. Rincón, and C. Torres, Urbach tail, disorder, and localized modes in ternary semiconductors, Phys. Rev. B **69**, 195201 (2004).

[65] F. Giustino, Electron-phonon interactions from first principles, Rev. Mod. Phys. **89**, 015003 (2017).

[66] F. Cerdeira, T. A. Fjeldly, and M. Cardona, Effect of free carriers on zone-center vibrational modes in heavily doped *p*-type Si. II. optical modes, Phys. Rev. B **8**, 4734 (1973).

[67] S. Pittala and S. Srinath, Effect of synthesis route on the multiferroic properties of $BiFeO_3$: A comparative study between solid state and sol–gel methods, J. Alloys Compd. **649**, 843 (2015).

[68] N. Izyumskaya, Y. Alivov, S. Cho, H. Morko, H. Lee, and Y. Kang, Processing, structure, properties, and applications of PZT thin films, Crit. Rev. Solid State Mater. Sci. **32**, 111 (2007).

[69] H. Chong, J. Liu, W. Yang, Q. Wu, H. Yang, and X. Xue, Photocatalytic activity of $CaTiO_3$ synthesized by solid state, sol–gel and hydrothermal methods, J. Sol-Gel Sci. Technol. **81**, 806 (2017).

[70] W. Jo, J. Kee, K. Kim, E. C. Landahl, G. Longbons, D. A. Walko, H. Wen, D. R. Lee, and S. Lee, Structural measurement of electron-phonon coupling and electronic thermal transport across a metal-semiconductor interface, Sci. Rep. **12**, 16606 (2022).

[71] W. Huang, W. Qian, M. A. El-Sayed, Y. Ding, and Z. L. Wang, Effect of the lattice crystallinity on the electron-phonon relaxation rates in gold nanoparticles, J. Phys. Chem. C **111**, 10751 (2007).

[72] A. Kumar, M. K. Warshi, A. Sagdeo, and P. R. Sagdeo, Investigations on the electronic structure of the strongly correlated electron system Cr-doped $PrFeO_3$, J. Phys. Chem. C **125**, 14048 (2021).

[73] C. Q. Hu, F. F. Meng, M. Wen, Z. Q. Gu, J. Y. Wang, X. F. Fan, and W. T. Zheng, Relationship between dielectric coefficient and Urbach tail width of hydrogenated amorphous germanium carbon alloy films, Appl. Phys. Lett. **101**, 042109 (2012).

[74] M. C. Weber, M. Guennou, H. J. Zhao, J. Íñiguez, R. Vilarinho, A. Almeida, J. A. Moreira, and J. Kreisel, Raman spectroscopy of rare-earth orthoferrites $RFeO_3$ (R = La, Sm, Eu, Gd, Tb, Dy), Phys. Rev. B **94**, 214103 (2016).

[75] See Supplemental Material at http://link.aps.org/supplemental/10.1103/PhysRevB.110.235201 for (i) The 2d contour plot for $\xi(T, \Theta_E)$. Fixing the temperature T and varying Θ_e enables to realize the discussed dependence conveniently (supplemental_material_file-I.mp4). (ii) The same depiction of in form of an *x*-*y* plot (supplemental_material_file-II.mp4), where the impact of $\xi(T, \Theta_E)$ is mapped on the physical observables in form of $\Gamma(T)$ vs $E_U(T)$ plot. clearly, it is linear for smaller values of ξ, and the deviation from linear behavior is realizable for the case of higher Θ_E.

[76] H. Fu, Topological ferroelectric phases by mode-selective phonon excitation, Phys. Rev. B **98**, 134111 (2018).

[77] R. Akasegawa, H. Zen, K. Hachiya, K. Yoshida, T. Goto, T. Sagawa, and H. Ohgaki, Mode-selective excitation of an infrared-inactive phonon mode in diamond using mid-infrared free electron laser, Jpn. J. Appl. Phys. **60**, 102001 (2021).

[78] J. Xu, Y. Hu, and H. Bao, Quantitative analysis of nonequilibrium phonon transport near a nanoscale hotspot, Phys. Rev. Appl. **19**, 014007 (2023).